Unusual perpendicular anisotropy in Co_2TiSi films

Yunlong Jin[1,2] ⓘ**, Shah Valloppilly**[2]**, Parashu Kharel**[3]**, Rohit Pathak**[4]**, Arti Kashyap**[4]**, Ralph Skomski**[1,2] **and D J Sellmyer**[1,2]

[1] Department of Physics and Astronomy, University of Nebraska, Lincoln, NE 68588, United States of America
[2] Nebraska Center for Materials and Nanoscience, University of Nebraska, Lincoln, NE 68588, United States of America
[3] Department of Physics, South Dakota State University, Brookings, SD 57007, United States of America
[4] School of Basic Sciences, Indian Institute of Technology Mandi, HP 175001, India

E-mail: yunlongjin@huskers.unl.edu

CrossMark

Abstract

Thin films of Co_2TiSi on MgO are investigated experimentally and theoretically. The films were produced by magnetron sputtering on MgO(0 0 1) and have a thickness of about 100 nm. As bulk Co_2TiSi, they crystallize in the normal cubic Heusler ($L2_1$) structure, but the films are slightly distorted ($c/a = 1.0014$) and contain some antisite disorder. The films exhibit a robust perpendicular anisotropy of 0.5 MJ m^{-3}. This result is surprising for several reasons. First, surface and interface anisotropies are too small to explain perpendicular anisotropy in such rather thick films. Second, Co_2TiSi has a substantial magnetization and crystallizes in a cubic Heusler structure, so that conventional wisdom predicts a preferential magnetization direction in the film plane rather than perpendicular. Third, the lattice strain of 0.14% is unable to account for the perpendicular anisotropy. We explain the perpendicular anisotropy as a quasicubic symmetry breaking chemical-ordering effect promoted by the substrate.

(Some figures may appear in colour only in the online journal)

1. Introduction

Anisotropy is arguably the most intriguing intrinsic magnetic property, with far-reaching implications in modern technology. For example, perpendicular thin-film anisotropy is important for magnetic-recording and spin electronics applications [1–18]. Thin-film anisotropy research includes half-metallic Co-based full-Heusler alloys, such as Co_2TiSi [3–5, 7, 10, 19–26]. Perpendicular magnetic anisotropy (PMA) is relatively easy to create in ultrathin films, due to atomic-scale surface and interface contributions [1–5]. For example, interfacial PMA had previously been achieved in ultrathin films of Heusler-ordered Co_2FeAl and Co_2FeSi alloys on MgO [27–29]. Specifically, deposition of Co_2TiSi on GaAs(0 0 1) yields perpendicular anisotropy for film thicknesses up to 13.5 nm, probably due to

nanocluster formation [13]. However, thermal stability in nano-electronic devices requires PMA in thicker films [3, 5, 7].

With the exception of ultrathin films, PMA is very difficult to create in materials with cubic crystal structure, such as Co_2TiSi. The reason is that interface and surface anisotropies decrease as $1/t$, where t is the thickness of the magnetic layer [1, 24, 30]. Bulk anisotropies (K_1) do not suffer from this restriction, but they are very low in cubic crystals [31], so that shape anisotropy, $K_s = -\mu_o M_s^2/2$, yields an orientation of the magnetization vector in the film plane.

In this paper, we report the realization of PMA in hybrid thin films of 100 nm Co_2TiSi on MgO(0 0 1). The underlying net anisotropy constant of approximately 0.5 MJ m^{-3} is unexpectedly large for materials with a cubic crystal structure and cannot be explained by interface anisotropy.

J. Phys. D: Appl. Phys. **52** (2019) 035001

Y Jin *et al*

2. Methods

2.1. Experimental methods

A magnetron sputtering system with a base pressure of about 3×10^{-8} Torr was used to epitaxially grow a series of Co_2TiSi films on an atomically flat MgO (001) substrate. The samples were co-deposited from Co, Ti and Si targets under optimized deposition conditions: argon pressure 2×10^{-3} Torr, substrate temperature 873 K, DC power of 110 W for the Ti target, and RF powers of 94.5 W and 142.5 W for the Co and Si targets, respectively. The bulk Co_2TiSi sample was prepared by arc melting and subsequent melt spinning with a wheel speed of 30 m s^{-1}. The crystal structure and epitaxy of the films and ribbons were investigated by in-plane and out-of-plane x-ray diffraction (XRD) using Rigaku SmartLab and Bruker D8 Discover diffractometers with Cu Kα radiation (wavelength 1.5406 Å), and an FEI Tecnai Osiris (Scanning) transmission electron microscope (TEM). The elemental compositions of the samples were determined using the energy-dispersive x-ray spectroscopy (EDX) in FEI Nova NanoSEM450 and TEM. The magnetic properties were measured using a Quantum Design SQUID magnetometer (MPMS) and physical property measurement system (PPMS).

2.2. Theoretical methods

Our first-principle LSDA calculations employ the projected-augmented-wave method [32] as implemented in the *Vienna ab initio simulation package* (VASP) [33, 34]. The exchange and correlation effects are described using a generalized gradient approximation within the PBE scheme, and the spin–orbit coupling has been included to calculate magnetic anisotropy energy. An energy cutoff of 500 eV has been taken for the plane-wave basis set, and the total energy is converged to 10^{-7} eV. Experimental lattice parameters $a = b = c = 5.651$ Å were used and the Brillouin-zone integration was performed using 1331 k-points in irreducible Brillouin zone. The magnetoelastic anisotropy K_{me} and the magnetoelastic constant λ have been determined by comparing well-converged and self-consistently determined total energies for three orthogonal magnetization directions as a function of the uniaxial strain ε.

3. Thin-film structure

Bulk Co_2TiSi crystallizes in the normal cubic Heusler or L2$_1$ structure (space group Fm$\bar{3}$m), figure 1(a). Figures 1(b) and (c) are top views of the unit cells of Co_2TiSi (b) and of the MgO(001) substrate (c). The unit cells figures 1(b) and (c) have a lattice mismatch of about 4%, which indicates that Co_2TiSi is likely to undergo a slight tetragonal distortion, $a = b \neq c$. The corresponding crystal structure is the tetragonal D0$_{22}$ structure (space group I4/mmm), which contains the L2$_1$ structure as a special case ($a = b = c$). To describe D0$_{22}$ structures, it is customary to choose a unit cell of reduced size, characterized by the two lattice parameters $a' = a/\sqrt{2}$ and $c' = c$. The change from a to a' corresponds to rotation of the coordinate frame by 45° in the *a-b*-plane, and the gray area in figure 1(b) is the tetragonal unit cell viewed from above. Note that a' is also the lattice constant of the MgO substrate (c). However, for our purposes, it is convenient to stick with the tetragonally distorted L2$_1$ unit cell, where $a \approx c$. Figure 1(d) summarizes the real structure of the film, as deduced from experiment (see below). The layers close to the interface grow epitaxially in a strained D0$_{22}$ structure (light red), in a relaxation region, the epitaxial strain is relieved through edge dislocations (pink), and most of the film is L2$_1$ ordered with little or no strain (light blue).

3.1. X-ray diffraction (XRD)

Figure 2 shows the XRD patterns of bulk Co_2TiSi (a) and of a 100 nm-thick Co_2TiSi film deposited on MgO, measured out-of-plane (b). The structure is L2$_1$, as evident for example from the (111) and (200) superlattice peaks. In figure 2(b), the two prominent non-MgO peaks are the (002) and (004) Bragg reflections of Co_2TiSi, indicating that the films maintain the crystalline orientation of the MgO substrate. The lattice parameter of the bulk sample is $a = 5.729$ Å. The corresponding value for the MgO substrate, $a = 5.955$ Å ($a' = 4.211$ Å), yields a tetragonally distorted L2$_1$, or D0$_{22}$, structure with a lattice mismatch of 3.9% in the light red interface area in figure 1(c). However, the light-red and pink regions occupy only a small volume fraction of the film, about 5% (see below).

The thin-film Co_2TiSi, has the measured lattice parameters $a = 5.648$ Å and $c = 5.656$ Å. These lattice parameters largely correspond to the blue region in figure 1(d) and are somewhat smaller than the bulk a, which is probably due to off-stoichiometry. They correspond to a trivially small change in c/a ratio of only 0.14%, compared to the substrate-induced strain of the order of 3.9%.

The value of c is extracted from figure 2(b), whereas a is obtained from off-normal angle Bragg reflection. Figure 3 shows the XRD patterns of Co_2TiSi film collected at selected off-normal angles to obtain various Bragg reflections that are not accessible in the out-of-plane scans. The dashed red rectangular region demonstrates the existence of two distinct Bragg reflections at nearly the same scattering angle 2θ, but the two planes are nearly 30° tilted apart, figures 3(a) and (b). As detailed in (c), the corresponding (132) and (024) planes are unique to the D0$_{22}$ unit cell. The corresponding tetragonal unit cell ($a = 3.994$ Å and $c = 5.656$ Å) has been used for indexing Bragg reflections in figures 3(a) and (b).

### 3.2. Transmission electron microscopy

Further evidence in favor of epitaxial growth near the interface is provided by TEM analysis. Figure 4(a) shows the selected area electron diffraction (SAED) patterns and the corresponding indices for Co_2TiSi [110]. The presence of the (111) spot confirms the L2$_1$ order of the film. The corresponding lattice constants, obtained by SAED patterns, are same as those obtained by XRD. Figure 4(c) is a
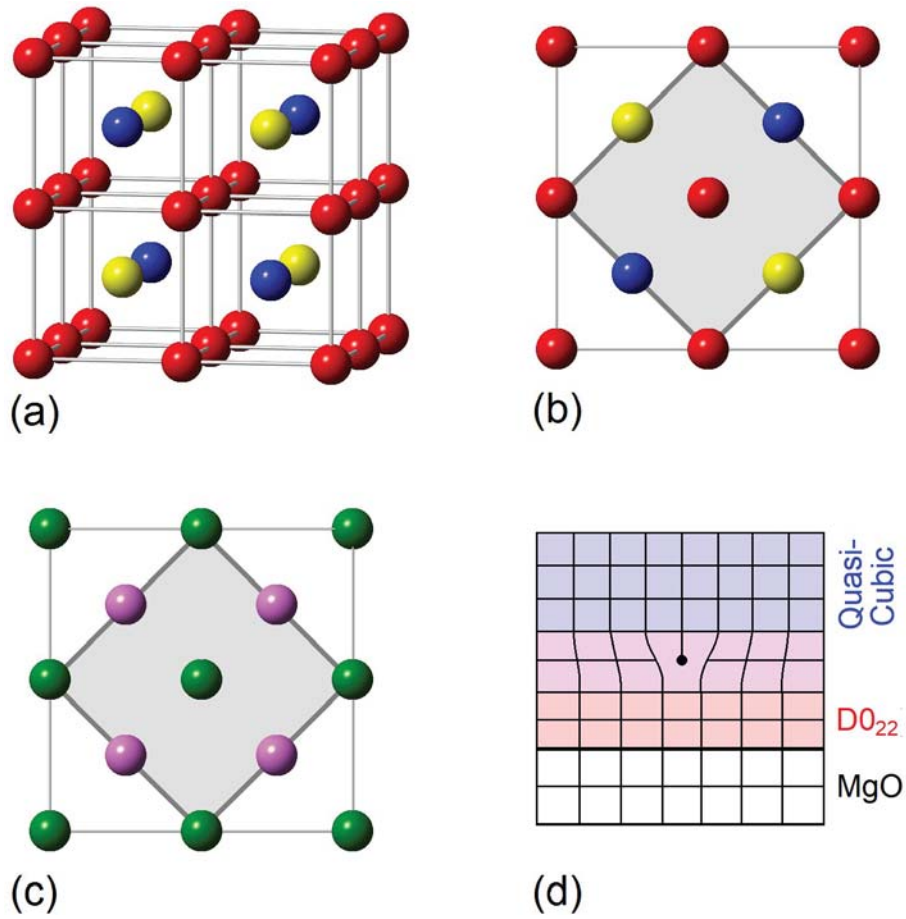
Figure 1. Crystal structures: (a) unit cell of $L2_1$-ordered Co_2TiSi, where red, yellow, and blue atoms are Co, Ti, and Si, respectively; (b) top view of the $L2_1$ unit cell; (c) top view of the unit cell of MgO(0 0 1), where the respective pink and green atoms are O and Mg; and (d) schematic side view of Co_2TiSi on MgO(0 0 1). The gray areas in (b) and (c) symbolize the unit cells of the tetragonal $D0_{22}$ structure (b) and of the cubic NaCl-ordered MgO (c). The $D0_{22}$ and NaCl structures are related to the $L2_1$ structure through a rotation by 45° and $a \rightarrow a' = a/\sqrt{2}$.
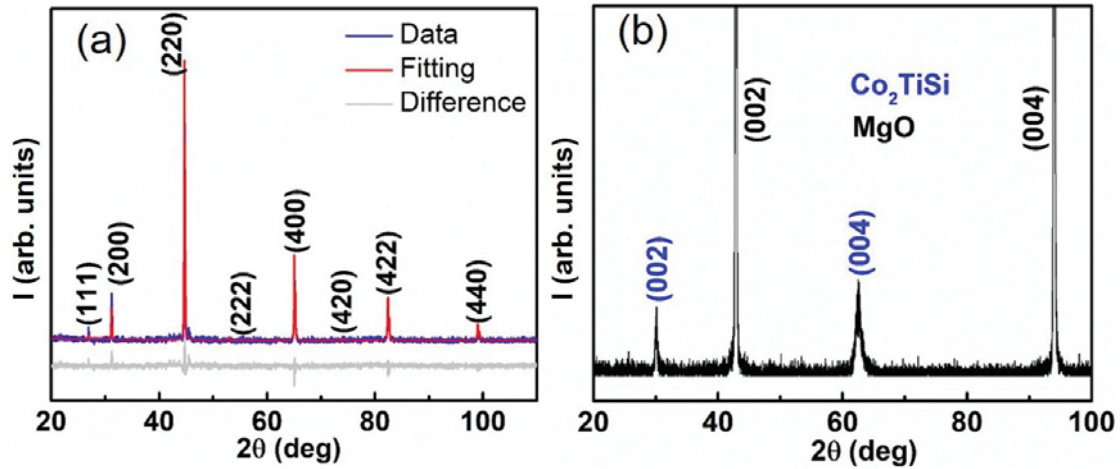
Figure 2. XRD patterns of Co_2TiSi: (a) bulk prepared by melt quenching process with Rietveld analysis based on $L2_1$ structure and (b) out-of-plane epitaxial thin-film on MgO(0 0 1).
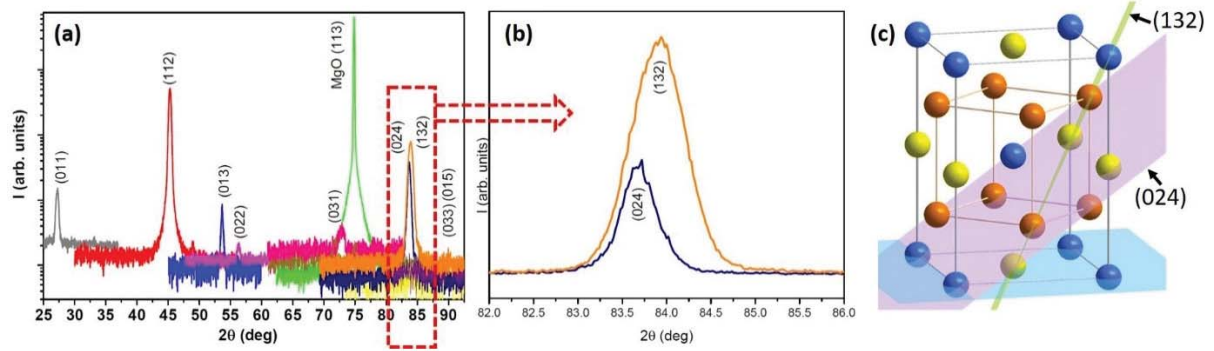
Figure 3. Off-normal angle Bragg reflection: (a) XRD patterns of Co_2TiSi film collected at selected off-normal angles to obtain various Bragg reflections that are not accessible in the out-of-plane scans, (b) expanded 2θ region of the $(0\,2\,4)$ and $(1\,3\,2)$ peaks, and (c) the $(0\,2\,4)$ and $(1\,3\,2)$ planes in the $D0_{22}$ unit cell.
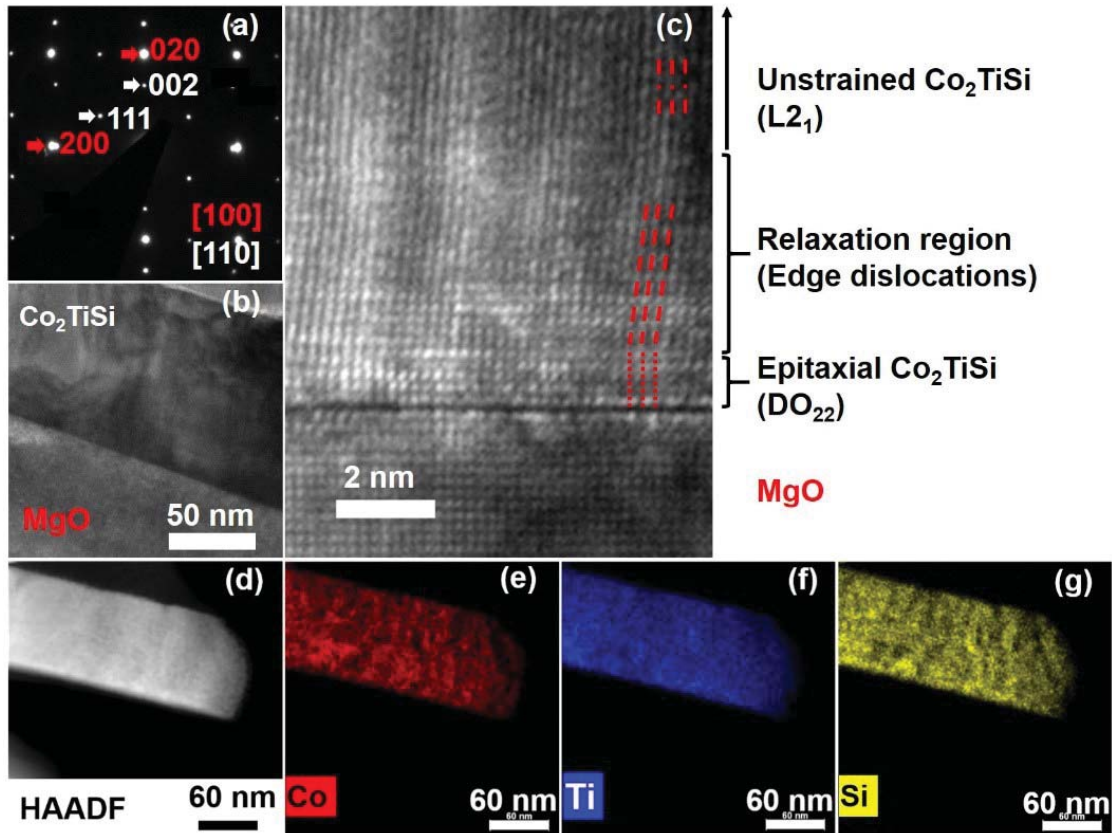
Figure 4. TEM analysis of the thin-film nanostructure: (a) SAED pattern and indexing of thin-film Co_2TiSi; (b) TEM image of both film and substrate, (c) high-resolution TEM image of the interface between film and substrate; (d)–(g) HAADF image showing the Z (atomic number) contrast and the corresponding EDS color maps.

high-resolution TEM image of the interface between Co_2TiSi and MgO. We see that there is epitaxial film growth and little lattice mismatch at the interface.

The TEM image of figure 4(b) shows that the Co_2TiSi layers have a thickness of about 100 nm. The composition of the films was investigated using scanning-TEM measurements (STEM). Figures 3(d)–(g) show a high-angle annular dark-field (HAADF) image of Co_2TiSi film with Z (atomic number) contrast maps and the corresponding energy-dispersive x-ray spectroscopy (EDS) color maps for Co, Ti and Si.

3.3. EDS analysis

Figure 5 presents a HAADF image of repeated Co_2TiSi film with Z (atomic number) contrast maps and the corresponding EDS color maps for Co, Ti and Si. The EDS analysis (figure 5(e)) indicates that the sample is somewhat Si lean, corresponding to $Co_2Ti_{1.27}Si_{0.88}$, which explains the slightly reduced lattice parameter compared to ideally stoichiometric bulk Co_2TiSi. In the meantime, the EDS line scan (figure 5(f)) along the green arrow from interface to surface

J. Phys. D: Appl. Phys. **52** (2019) 035001

Y Jin *et al*
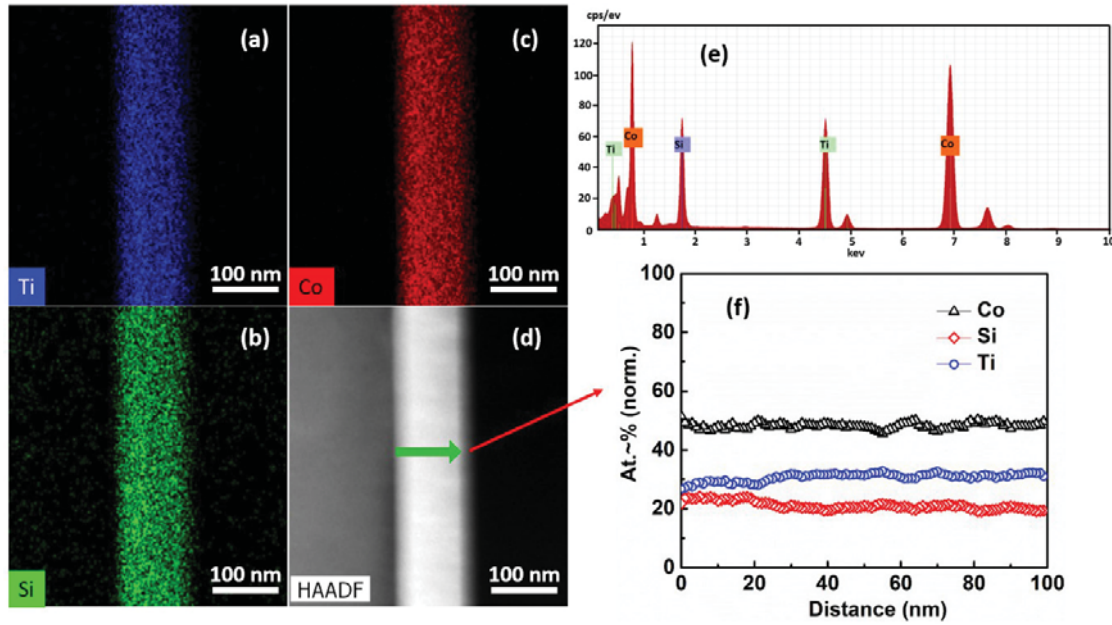
Figure 5. EDS color maps of the 100 nm thin-film: (a)–(d) The EDS color maps of repeated thin-film samples and the corresponding HAADF image showing the Z (atomic number) contrast; (e) The EDS spectrum of Co_2TiSi thin-film. (f) Atomic percentage of Co, Ti and Si results of EDS line scan along the green arrow as shown in (d).

shows that the sample is somewhat Si lean, corresponding to $Co_{48.2}Ti_{30.7}Si_{21.1}$ (d).

4. Magnetic properties

Figure 6 summarizes the magnetic properties of the film, showing the hysteresis loops at 5 K (a) and at 300 K (b), recorded in magnetic fields parallel and perpendicular to the film plane. The saturation magnetization $J_s = 0.5$ T [$M_s = 400$ emu cm^{-3}] corresponds to about 2.1 μ_B per formula unit, which agrees fairly well with the value of 2.0 μ_B predicted by the Slater–Pauling curve for the half-metallic phase of Co_2TiSi [25]. Figure 6(c) shows that the Curie temperature is slightly above room temperature, close to 320 K. This is a substantial improvement compared to Co_2TiSi on GaAs, where the Curie temperature is only about 28 K, and further improvements may be easily realized by Fe doping [35, 36].

Surprisingly, the films have pronounced perpendicular anisotropy, with low-temperature coercivities $\mu_o H_c$ of about 0.27 T [$H_c = 2.7$ kOe] for the out-of-plane field and 0.05 kOe for the in-plane field. The case normally expected for thin-film magnets with cubic crystal structures is a preferred magnetization direction in the film plane, as opposed to perpendicular to the film plane. Close to the Curie point, anisotropy and coercivity collapse, figure 6(b), which is a common feature of magnetic systems [31]. As shown in figures 6(e) and (f), by contrast, the melt-spun Co_2TiSi ribbons, the Curie temperature of which was measured to be 350 K, are isotropic and exhibit virtually no magnetic anisotropy even at low temperatures.

The magnetic anisotropy has been estimated from the in-plane curve (blue) in figure 6(a). Extrapolating the linear part of the curve to the saturation magnetization yields a low-temperature anisotropy field $H_a = 2K_{eff}/J_s$ [31, 37] of about 20 dT and $K_{eff} = 0.4$ MJ m^{-3}. To analyze this value, we decompose the effective anisotropy

$$K_{eff} = K_1 + K_s/t - K_{sh} \tag{1}$$

into magnetocrystalline ($K_1 = K_u$), interface and surface (K_s), and shape (K_{sh}) anisotropy contributions, where t is the thickness of the magnetic layer. Perpendicular anisotropy means that $K_1 + K_s/t$ must be larger than $K_{sh} \approx 0.1$ MJ m^{-3} for the present material. The magnitudes of surface and interface anisotropies are not much larger 0.1 to 1 mJ m^{-2} [31, 37]. According to equation (1), the K_s value must be divided by $t = 100$ nm, which is thick by atomic standards and yields $K_s/t \approx 0.001$ to 0.01 MJ m^{-3}. Figure 6(d) shows the corresponding experimental analysis for the films at 5 K. Plotting $K_{eff}t$ as a function of the film thickness yields $K_s = 1.29$ mJ m^{-2} from the vertical-axis intercept of the dashed line. This value is comparable to that of other Heusler films on MgO [29]. The figure confirms that the surface and interface anisotropy contribution is indeed negligible. The slope of the red line in figure 6(d) yields $K_{eff} \approx 0.40$ MJ m^{-3}, which corresponds to $K_1 \approx 0.50$ MJ m^{-3}.

4.1. Origin of perpendicular anisotropy

Magnetocrystalline anisotropies in cubic iron-series transition-metal intermatallics are typically of the order of $|K_1| = 0.005$ to 0.05 MJ m^{-3} [38]. There are two basic ways of creating such uniaxial (noncubic) anisotropies, namely by deforming the cubic unit cell (magnetoelastic anisotropy) [31, 37] or by keeping the cubic unit cell and repositioning the atoms in the cell (pseudocubic anisotropy).

J. Phys. D: Appl. Phys. **52** (2019) 035001

Y Jin *et al*
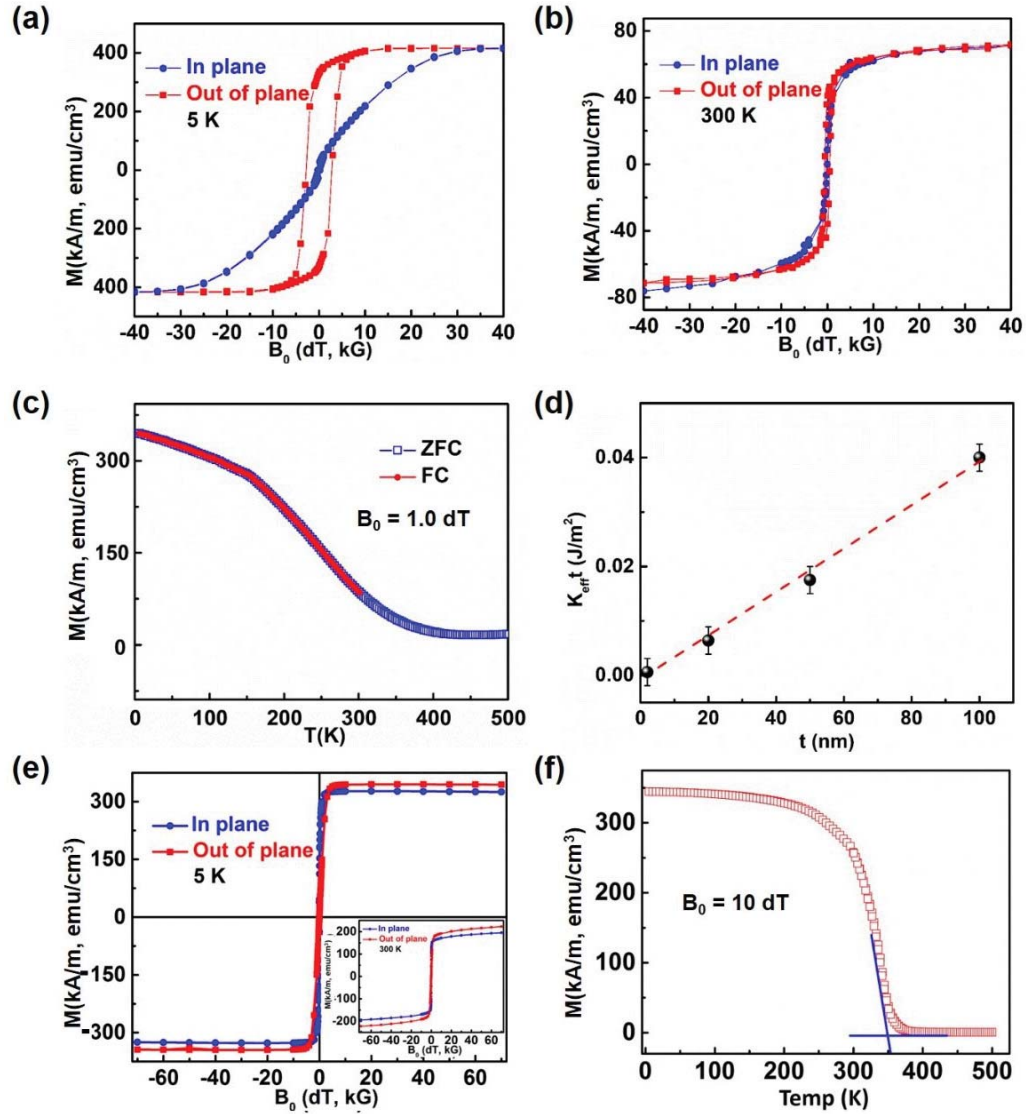
Figure 6. Magnetization of Co_2TiSi as a function of external magnetic field and temperature: (a) thin-film hysteresis loops at 5 K, (b) thin-film hysteresis loops at 300 K, (c) field-cooled (FC) and zero-field-cooled (ZFC) thin-film magnetization curves in a field of 1.0 dT [1 kOe], and (d) thickness dependence of the product of $K_{eff}t$ of Co_2TiSi thin films at 5 K, (e) melt-spun ribbons of Co_2TiSi hysteresis loops at 5 K and 300 K, (f) temperature dependence of magnetization curve of ribbons in a field of 10 dT.

The effect of substrate-induced strain is of the order of $K_{me} = 3\lambda_s\varepsilon Y/2$, where λ_s is the saturation magnetostriction, ε is the uniaxial strain, and Y is Young's modulus. To determine λ_s, we have used density-functional calculations. Based on $\varepsilon = 0.04$ and $Y = 100\,GPa$ for Co_2TiSi, we estimate $\lambda_s \approx 100 \times 10^{-6}$, which is in the range expected for iron-series transition-metal magnets [31].

Based on a c/a ratio of 1.04, our density-functional (DFT) anisotropy calculations yield a low-temperature anisotropy of magnitude 0.45 MJ m^{-3}. However, such high strains and anisotropy contribution are limited to the interface region, light red and pink areas in figure 1(d). Figure 4(c) suggests epitaxial and relaxation regions of about 1.6 nm and 4 nm, respectively, which occupy only about 5 nm of the 100 nm film, corresponding to a net anisotropy contribution of 0.02 MJ m^{-3}. In the main part of the film, namely in the light blue region of figure 1(d), $c/a = 1.0014$, which yields a net anisotropy contribution of only about 0.015 MJ m^{-3}.

The anisotropy of our Co_2TiSi films is probably of the *pseudo-cubic* type. This type of anisotropy arises in magnets where $a = b = c$ but the arrangement of the atoms inside the unit cells breaks the cubic symmetry. Experimentally well-investigated examples are $L1_0$ magnets such as FePt and CoPt, where $a = b \approx c$ [31, 39, 40] and a small strain can be used to realize $c/a = 1$ without substantial change in the high magnetic anisotropy. Pseudocubic anisotropy has not been observed yet in Heusler alloy, although the B2 structures theoretically investigated by Hirohata *et al* [40] contain a super-structure (figure 12 in [40]) and may therefore be classified as pseudocubic magnets.

J. Phys. D: Appl. Phys. **52** (2019) 035001

Y Jin *et al*
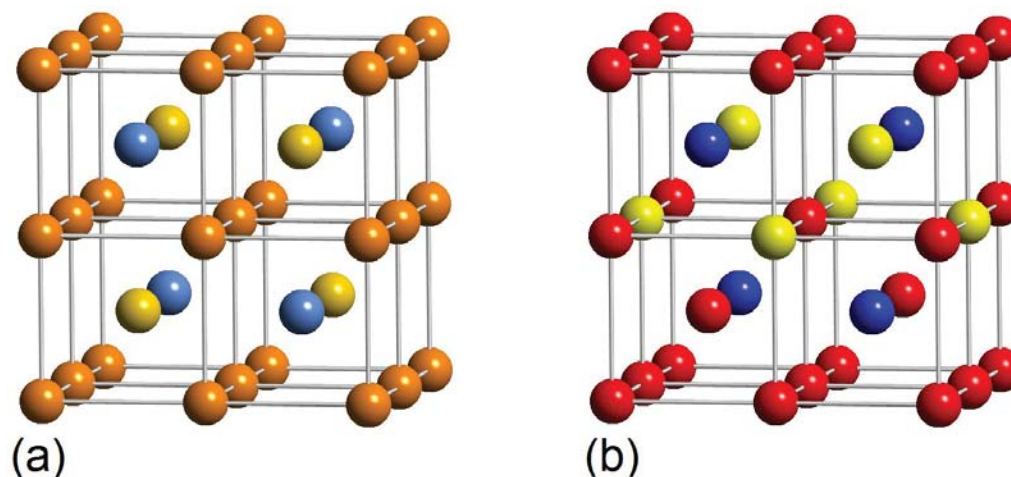
Figure 7. Chemical disorder in pseudocubic Co_2TiSi thin films: (a) average site occupancies according to Rietveld analysis (dark orange: $Co_{85}Ti_{15}$, light orange: $Ti_{70}Co_{30}$, light blue: 65% Si) and (b) example of a chemically disordered unit cells having two antisite defects. As elsewhere in the paper, red, yellow, and blue atoms denote Co, Ti, and Si, respectively.

In the present system, pseudocubic *c*-axis anisotropy is possible due to the influence of the MgO substrate. In section 3, we have shown that the strain relaxes in the main part of the film, but this does not necessarily mean that cubic symmetry is restored. For example, some noncubic atomic 'pair' or 'planar' order may survive, the latter being similar to that observed in $L1_0$ magnets. We do not have an unambiguous proof for pseudocubic anisotropy, but several experimental and theoretical arguments speak in favor of this mechanism. Experimentally, an XRD intensity analysis of several Bragg reflections of thin-film samples suggests that 30% of Co and Ti exchange the positions between their nominal sites as well as the 4*a* sites being Si lean (65% occupancy). This situation is depicted in figure 7(a), where light blue indicates partial Si occupancy and different shades of orange indicate intermediate average occupancies by Co (red) and Ti (yellow).

While our XRD analysis is not able to unambiguously prove that the system undergoes a symmetry breaking due to chemical order, the 'orange' occupancies in figure 7(a) reflect antisite disorder involving Co and Ti atoms. These antisite Co–Ti pairs are likely to exhibit some orientational preferences due to the influence of the substrate. Note that the *c/a* ratio is slightly larger than one, which speaks in favor of a chemical-ordering effect. If the *c/a* ratio was caused by residual unrelaxed strain, it would be smaller than one, because the lattice constant of the MgO substrate is bigger than *a* of the thin-film Co_2TiSi. Further evidence for chemical inhomogeneity in the perpendicular direction comes from figure 5(f), which indicates a substantial variation of the chemical composition as a function of the distance from the interface. In particular, the Si-to-Ti ratio systematically decreases with increasing distance from the interface.

As an explicit example, we have used DFT to evaluate the atomic configuration of figure 7(b) and obtained a magnetic anisotropy of 0.49 meV per antisite defect, corresponding to about 0.43 MJ m^{-3} if one assumes one effective antisite defect per 16-atom unit cell. This example show that chemical disorder reproduces the right order of magnitude of the magnetic anisotropy.

5. Conclusions

In summary, we have created robust PMA of about 0.5 MJ m^{-3} in a hybrid structure of 100 nm Co_2TiSi on MgO(001). Neither strain nor interface or surface anisotropies can explain this unusual behavior, which we attribute to pseudocubic chemical order initiated by the MgO substrate. Our approach shows how thin-film processing can be used to create PMA and may open a new pathway towards materials-by-design for spin electronics. Future research is necessary on the anisotropy of Co_2TiSi and related Heusler alloys.

ORCID iDs

Yunlong Jin ⓘ https://orcid.org/0000-0003-1946-8474

References

[1] Maruyama T *et al* 2009 Large voltage-induced magnetic anisotropy change in a few atomic layers of iron *Nat. Nanotechnol.* **4** 158–61
[2] Mathon J and Umerski A 2001 Theory of tunneling magnetoresistance of an epitaxial Fe/MgO/Fe(001) junction *Phys. Rev.* B **63** 220403
[3] Dieny B and Chshiev M 2017 Perpendicular magnetic anisotropy at transition metal/oxide interfaces and applications *Rev. Mod. Phys.* **89** 025008

J. Phys. D: Appl. Phys. **52** (2019) 035001

Y Jin *et al*

[4] Mitani S 2016 Magnetic tunnel junctions using Heusler alloys *Heusler Alloys: Properties, Growth, Applications* (Berlin: Springer)

[5] Wen Z *et al* 2014 A 4-fold-symmetry hexagonal ruthenium for magnetic heterostructures exhibiting enhanced perpendicular magnetic anisotropy and tunnel magnetoresistance *Adv. Mater.* **26** 6483–90

[6] Liu T, Zhang Y, Cai J W and Pan H Y 2014 Thermally robust Mo/CoFeB/MgO trilayers with strong perpendicular magnetic anisotropy *Sci. Rep.* **4** 5895

[7] Nozaki T *et al* 2010 Voltage-induced perpendicular magnetic anisotropy change in magnetic tunnel junctions *Appl. Phys. Lett.* **96** 022506

[8] Nakamura K *et al* 2009 Giant modification of the magnetocrystalline anisotropy in transition-metal monolayers by an external electric field *Phys. Rev. Lett.* **102** 187201

[9] Weisheit M *et al* 2007 Electric field-induced modification of magnetism in thin-film ferromagnets *Science* **315** 349–51

[10] Chappert C, Fert A and Van Dau F N 2007 The emergence of spin electronics in data storage *Nat. Mater.* **6** 813–23

[11] Yang H *et al* 2016 Anatomy and giant enhancement of the perpendicular magnetic anisotropy of Cobalt–graphene heterostructures *Nano Lett.* **16** 145–51

[12] Schellekens A J *et al* 2012 Electric-field control of domain wall motion in perpendicularly magnetized materials *Nat. Commun.* **3** 847

[13] Sahota P K *et al* 2012 Ultrahard magnetic nanostructures *J. Appl. Phys.* **111**

[14] Miron I M *et al* 2011 Perpendicular switching of a single ferromagnetic layer induced by in-plane current injection *Nature* **476** 189–94

[15] Wolf S A *et al* 2010 The promise of nanomagnetics and spintronics for future logic and universal memory *Proc. IEEE* **98** 2155–68

[16] Ikeda S *et al* 2010 A perpendicular-anisotropy CoFeB–MgO magnetic tunnel junction *Nat. Mater.* **9** 721–4

[17] Heinonen O G and Dimitrov D V 2010 Switching-current reduction in perpendicular-anisotropy spin torque magnetic tunnel junctions *J. Appl. Phys.* **108** 014305

[18] Andreas M *et al* 2002 Magnetic recording: advancing into the future *J. Phys. D: Appl. Phys.* **35** R157

[19] Dau M T, Jenichen B and Herfort J 2015 Perpendicular magnetic anisotropy in the Heusler alloy Co_2TiSi/GaAs(0 0 1) hybrid structure *AIP Adv.* **5** 057130

[20] Dau M T and Herfort J 2015 Molecular beam epitaxy growth and properties of Co_2TiSi thin films on GaAs(0 0 1): the effect of growth temperature *J. Phys. D: Appl. Phys.* **48** 025003

[21] Yu G *et al* 2014 Switching of perpendicular magnetization by spin–orbit torques in the absence of external magnetic fields *Nat. Nanotechnol.* **9** 548–54

[22] Koo J W *et al* 2013 Large perpendicular magnetic anisotropy at Fe/MgO interface *Appl. Phys. Lett.* **103** 192401

[23] Garello K *et al* 2013 Symmetry and magnitude of spin–orbit torques in ferromagnetic heterostructures *Nat. Nanotechnol.* **8** 587–93

[24] Wang W-G, Li M, Hageman S and Chien C L 2011 Electric-field-assisted switching in magnetic tunnel junctions *Nat. Mater.* **11** 64–8

[25] Joachim Barth G H F, Balke B and Felser C 2011 Anomalous transport properties of the half-metallic ferromagnets Co_2TiSi, Co_2TiGe and Co_2TiSn *Phil. Trans. R. Soc.* A **369** 3588–601

[26] Mangin S *et al* 2006 Current-induced magnetization reversal in nanopillars with perpendicular anisotropy *Nat. Mater.* **5** 210–5

[27] Phatak C, Heinonen O, De Graef M and Petford-Long A 2016 Nanoscale Skyrmions in a nonchiral metallic multiferroic: Ni_2MnGa *Nano Lett.* **16** 4141–8

[28] Takamura Y, Suzuki T, Fujino Y and Nakagawa S 2014 Full-Heusler Co_2FeSi alloy thin films with perpendicular magnetic anisotropy induced by MgO-interfaces *J. Appl. Phys.* **115** 17C732

[29] Wen Z, Sukegawa H, Mitani S and Inomata K 2011 Perpendicular magnetization of Co_2FeAl full-Heusler alloy films induced by MgO interface *Appl. Phys. Lett.* **98** 242507

[30] Duan C-G *et al* 2008 Surface magnetoelectric effect in ferromagnetic metal films *Phys. Rev. Lett.* **101** 137201

[31] Skomski R 2008 *Simple Models of Magnetism* (Oxford: Oxford University Press)

[32] Kresse G and Joubert D 1999 From ultrasoft pseudopotentials to the projector augmented-wave method *Phys. Rev.* B **59** 1758–75

[33] Kresse G and Furthmüller J 1996 Efficient iterative schemes for *ab initio* total-energy calculations using a plane-wave basis set *Phys. Rev.* B **54** 11169–86

[34] Kresse G and Furthmüller J 1196 Efficiency of *ab initio* total energy calculations for metals and semiconductors using a plane-wave basis set *Comput. Mater. Sci.* **6** 15–50

[35] Jin Y *et al* 2017 Effect of Fe substitution on the structural, magnetic and electron-transport properties of half-metallic Co_2TiSi *AIP Adv.* **7** 055812

[36] Engdahl G and Bright C B 2000 Chapter 3—magnetostrictive design *Handbook of Giant Magnetostrictive Materials* (San Diego: Academic)

[37] Coey J M D 2010 *Magnetism and Magnetic Materials* (Cambridge: Cambridge University Press)

[38] Skomski R 2003 Nanomagnetics *J. Phys.: Condens. Matter.* **15** R841

[39] Klemmer T, Hoydick D, Okumura H, Zhang B and Soffa W A 1995 Magnetic hardening and coercivity in L10 ordered FePd ferromagnets *Scr. Met. Mater.* **33** l793–805

[40] Hirohata A *et al* 2017 Development of antiferromagnetic Heusler alloys for the replacement of iridium as a critically raw material *J. Phys. D: Appl. Phys.* **50** 443001